



HAL
open science

Ultrasound Contrast Imaging: Influence of Scatterer Motion in Multi-pulse Techniques

Fanglue Lin, Christian Cachard, Riccardo Mori, François Varray, Francesco Guidi, Olivier Basset

► **To cite this version:**

Fanglue Lin, Christian Cachard, Riccardo Mori, François Varray, Francesco Guidi, et al.. Ultrasound Contrast Imaging: Influence of Scatterer Motion in Multi-pulse Techniques. IEEE Transactions on Ultrasonics, Ferroelectrics and Frequency Control, 2013, 60 (10), pp.2065-2078. 10.1109/TUFFC.2013.2797 . hal-01957677

HAL Id: hal-01957677

<https://hal.science/hal-01957677v1>

Submitted on 29 Jan 2025

HAL is a multi-disciplinary open access archive for the deposit and dissemination of scientific research documents, whether they are published or not. The documents may come from teaching and research institutions in France or abroad, or from public or private research centers.

L'archive ouverte pluridisciplinaire **HAL**, est destinée au dépôt et à la diffusion de documents scientifiques de niveau recherche, publiés ou non, émanant des établissements d'enseignement et de recherche français ou étrangers, des laboratoires publics ou privés.



Distributed under a Creative Commons Attribution - NonCommercial 4.0 International License

Ultrasound Contrast Imaging: Influence of Scatterer Motion in Multi-Pulse Techniques

Fanglue Lin, Christian Cachard, Riccardo Mori, François Varray, Francesco Guidi, and Olivier Basset

Abstract—In ultrasound contrast imaging, many techniques based on multiple transmissions have been proposed to increase the contrast-to-tissue ratio (CTR). They are generally based on the response of static scatterers inside the imaged region. However, scatterer motion, for example in blood vessels, has an inevitable influence on multi-pulse techniques, which can either enhance or degrade the technique involved. This paper investigates the response of static nonlinear media insonated by multi-pulses with various phase shifts, and the influence of scatterer motion on multi-pulse techniques. Simulations and experimental results from a single bubble and clouds of bubbles show that the phase shift of the echoes backscattered from bubbles is dependent on the transmissions’ phase shift, and that the bubble motion influences the efficiency of multi-pulse techniques: fundamental and second-harmonic amplitudes of the processed signal change periodically, exhibiting maximum or minimum values, according to scatterer motion. Furthermore, experimental results based on the second-harmonic inversion (SHI) technique reveal that bubble motion can be taken into account to regulate the pulse repetition frequency (PRF). With the optimal PRF, the CTR of SHI images can be improved by about 12 dB compared with second-harmonic images.

I. INTRODUCTION

ULTRASOUND contrast agents (UCAs) are suspensions of microbubbles injected into human blood vessels. They can pass through the lung capillary circulation and are stable, therefore increasing the bubble lifetime. Most of them have diameters less than 10 μm . The development of UCA was motivated at first by its high echogenicity and was used to enhance the backscattered signals from the blood pool, leading to a better discrimination between blood and tissue [1]. Then it was found that bubbles, if properly excited, also backscattered harmonics because of their nonlinear vibration [2], [3]. If the tissue can be con-

sidered as linear reflectors, then harmonic imaging was naturally proposed to observe the behavior of blood. In particular, second-harmonic imaging remains the commonly adopted technique, in accordance with the limited bandwidth of traditional transducers.

However, it was observed that the transmitted wave is gradually deformed during the propagation in tissue and then also generates harmonics [4]. The tissue can be approximated to a linear system only when low acoustic pressures are taken into account. Therefore, the contrast-to-tissue ratio (CTR) is limited because of the native tissue-generated harmonics. Eq. (1) presents the definition of the CTR_n , used to quantify the extent of discrimination between UCA and tissue at a specific harmonic:

$$\text{CTR}_n = 20 \log \frac{P_n^{\text{UCA}}}{P_n^{\text{tissue}}}, \quad (1)$$

where P_n^{UCA} and P_n^{tissue} are backscattered pressures of the n th harmonic from UCA and tissue, respectively. Conventionally, the second harmonic is considered. Recently, other harmonics have also been used, for example in sub-harmonic imaging [5] or in super-harmonic imaging [6].

Eq. (1) indicates that to increase CTR, the tissue response should be reduced and/or the bubble response should be enhanced.

To increase CTR by reducing tissue response, some single-pulse techniques have been proposed. Several techniques used the idea of source pre-biasing to increase CTR_2 by suppressing the tissue-generated second harmonics [7]–[11]. The differences between these techniques lie in how the source pre-biasing signal is designed. Shen *et al.* proposed a technique transmitting a fundamental and a phase-shifted third-harmonic wave simultaneously to cancel the second harmonic [12], [13]. The same group also used the harmonic leakage signal to produce the second-harmonic reduction signal [14], [15].

All of the aforementioned methods are single-pulse techniques, and many multi-pulse techniques have also been proposed to increase the CTR. The most common multi-pulse technique is called pulse inversion (PI) [16]. A sequence of two inverted pulses is transmitted and the two received signals are summed. For a linear system (such as tissue insonified by low acoustic pressures), the response of the second pulse is an inverted copy of the response from the first pulse and the sum of the two pulses is zero. For a nonlinear system (such as bubbles and tissue insoni-

This work was funded by the ANR-11 TecSan-008-01 BBMUT and was supported by the LABEX CeLyA (ANR-10-LABX-0060) of Université de Lyon, within the program “Investissements d’Avenir” (ANR-11-IDEX-0007) operated by the French National Research Agency (ANR).

F. Lin, C. Cachard, F. Varray, and O. Basset are with the Centre de Recherche en Acquisition et Traitement de l’Image pour la Santé (CREATIS), CNRS UMR 5220, INSERM U1044, Institut National des Sciences Appliquées de Lyon (INSA Lyon), Université Lyon 1, Villeurbanne, France (e-mail: fanglue.lin@creatis.insa-lyon.fr).

R. Mori is with the Physikalisches Institut, Albert-Ludwigs-Universität Freiburg, Freiburg, Germany.

F. Guidi is with the Microelectronics Systems Design Laboratory, Università di Firenze, Florence, Italy.

fied by high acoustic pressures), the sum is not zero. In fact, PI not only improves CTR, but also overcomes the trade-off of contrast detectability and imaging resolution [17]. However, in actual ultrasound systems, a second-harmonic band-pass filter is usually applied to remove the residual fundamental components.

Pasovic *et al.* proposed a multi-pulse method called second-harmonic inversion (SHI¹) [18]. As in PI, a sequence of two pulses is transmitted and the two responses are summed; however, the phase shift between the two transmitted pulses is 90°. Then, the second harmonic is filtered to form a SHI image. Because the second-harmonic component has a quadratic relationship to the fundamental component, the phase shift between the two second-harmonic components is 180°, so the second harmonic of the summed signal is canceled in tissue. In the UCA region, preservation of the second harmonic was observed (the maximum reduction was only 0.3 dB), therefore, CTR₂ is effectively increased. The preservation of the second harmonic in UCA was explained, based on the observation of Morgan *et al.*, by the fact that the phase of reflected signals from a single bubble excited by two inverted single-cycle pulses was not significantly changed [19]. However, this preservation can be induced by the motion of the bubbles, considering that the UCA were always stirred during the acquisitions.

Besides PI and SHI, there are also several methods using multiple transmissions which are intended to increase the nonlinear response of microbubbles. Brock-Fisher *et al.* used an amplitude modulation (AM) technique [20]. The linear echoes were canceled, but some of the nonlinear components were still preserved within the probe bandwidth. The combination of phase and amplitude modulation in a more generalized nonlinear detection process was first suggested by Haider and Chiao [21]. Eckersley *et al.* combined PI and AM in a technique in which the second pulse was inverted and had half the amplitude of the first pulse [22]. The response to the second pulse was multiplied by two before the summation with the response to the first pulse. The bubble-scattered signal was enhanced by 4 ± 1 dB. Wilkening *et al.* transmitted five pulses with equidistant phases, a weighted summation of the received echoes allowed the suppression of the selective harmonics [23], [24].

Although a large number of studies have provided excellent work on estimating the models of a vibrating bubble [25], [26] and the models of ultrasound propagation through contrast media [27], few studies have been presented on the alteration of the UCA backscattered signal according to phase-shifted transmissions. In fact, the literature reveals several conflicts: some authors believe that the bubble-scattered echo phase is not altered by a change in the transmitted signal phase [18], [19], whereas others consider the bubble-scattered echo phase to be altered by

¹Here, SHI does not refer to second-harmonic imaging, super-harmonic imaging, or sub-harmonic imaging, as used in some other studies.

the phase-shifted transmissions [16], [22]. This point is of major importance for multi-pulse techniques.

Furthermore, all multi-pulse techniques are influenced by scatterer motion during the pulse repetition interval (PRI). Note that the PRI is the reciprocal of the pulse repetition frequency (PRI = 1/PRF). Because the motion of the scatterers has the same effect as a phase shift, these motions can enhance or degrade the techniques involved. Therefore, the quantification of the influence of moving UCA insonated by multi-pulses is useful. This paper investigates not only the response of static nonlinear media insonated by multi-pulses with different phase shifts, but also the influence of scatterer motion on multi-pulse techniques.

The paper is organized as follows: Section II introduces the theoretical background of nonlinear wave propagation and the influence of scatterer motion; Section III presents the simulation results on a nonlinear medium with or without motion; Section IV presents the experimental results on a static tissue-mimicking phantom and circulating UCA; Section V discusses several problems and a preliminary approach, based on bubble motion, to optimize the SHI technique is proposed; and Section VI concludes this paper.

II. THEORY

A. Multi-Pulse Transmission With Static Scatterers

In multi-pulse transmission techniques, several waves are transmitted successively. The basic waveform of the transmitted waves is assumed to be

$$p_0(z = 0, t) = P_0 \cos(\omega_0 t + \varphi_0), \quad (2)$$

where P_0 is the amplitude of the wave, ω_0 is the angular frequency, φ_0 is the phase, and z is the propagation distance.

Suppose N is the number of transmitted waves, and b^k is a complex parameter indicating the relationship between the k th transmitted wave and the basic waveform [21]:

$$b^k = |b^k| e^{j\Delta\varphi^k}, \quad j^2 = -1, \quad \Delta\varphi^k \in [0, 2\pi], \quad k = 1, 2, \dots, N. \quad (3)$$

Then, the pressure wave of the k th transmitted wave is given as

$$p^k(z = 0, t) = |b^k| P_0 \cos(\omega_0 t + \varphi_0 + \Delta\varphi^k). \quad (4)$$

That is, the phase of the k th transmitted wave is

$$\varphi^k = \varphi_0 + \Delta\varphi^k. \quad (5)$$

After forward-and-back propagation of the pressure wave in the medium, because of the presence of harmonics either

from nonlinear propagation or from nonlinear scattering of the bubbles, the received pressure wave is expressed as

$$r^k(z = 0, t) = \sum_{n=1}^{\infty} \alpha_n^k \cos(n(\omega_0 t + \varphi^k)), \quad (6)$$

where α_n^k is the factor of the n th harmonic. The expression of α_n^k is not detailed here. It is a complex term depending on the media (tissue or bubbles), and on the frequency and amplitude of the propagating wave. In our case, it can be assumed that: 1) for the N phase-shifted waves transmitted with the same amplitude and frequency, and propagating in the same media, the value of α_n^k is the same (time-invariant); and 2) the phase shift of the n th harmonics of the received wave is n times the transmitted phase shift. In the discussion part, these assumptions are compared with the experimental results.

In a multi-pulse technique, the imaging signal is a weighted sum of the received signals from the N transmissions. c^k is defined as the weighting factor for the received signal from the k th transmission. Then the summation of these received waves can be expressed as

$$r_{\text{sum}}(z = 0, t) = \sum_{k=1}^N \left(c^k \sum_{n=1}^{\infty} \alpha_n^k \cos(n(\omega_0 t + \varphi^k)) \right). \quad (7)$$

Eq. (7) is the general expression of the weighted sum of N pulses propagating in the medium and backscattered to the probe.

B. Influence of Scatterer Motion

In multi-pulse techniques, media motion is inevitable during the PRI. Therefore, for multi-pulse transmissions with low media motions in the direction of transmitted wave propagation, (4) can be written as

$$p^k(z = 0, t) = |b^k| P_0 \cos(\omega_0 t + \varphi_0 + \Delta\varphi^k + \theta^k), \quad (8)$$

where θ^k is the scatterer motion expressed as an additional phase shift of the transmitted wave:

$$\theta^k = \frac{4\pi\Delta z^k}{\lambda}. \quad (9)$$

Δz^k is the scatterer motion during the time interval between the first and k th transmitted wave. λ is the wavelength of the transmitted waves. Assuming the velocity v of the moving scatterers is constant,

$$\Delta z^k = (k - 1)\text{PRI} \cdot v = (k - 1) \frac{v}{\text{PRF}}. \quad (10)$$

Then, the final effect depends on the combination of transmitted phase shifts and motions. The additional phase shift (9) becomes

$$\theta^k = (k - 1) \frac{4\pi v}{\lambda \cdot \text{PRF}}. \quad (11)$$

This additional phase shift influences the efficacy of multi-pulse techniques. With suitable scatterer motion, the efficiency of multi-pulse techniques can be enhanced.

III. SIMULATION

To simulate the media response to transmitted pulses with various phase shifts and the influence of media motion to multi-pulse techniques, the simulator CREANUIS was used [28]. This tool simulates nonlinear RF ultrasound images containing both the fundamental and the second-harmonic evolution.

A collection of randomly distributed scatterers was simulated as a homogeneous medium. The nonlinear coefficient β of this medium was 4.5, corresponding to a typical biological medium [29], [30].

The transmitted 4-cycle waves had a central frequency of 2 MHz and an initial pressure of 200 kPa. The simulated aperture was 15.4 mm, the image depth was 80 mm, and the focal depth was 70 mm. One RF frame consisting of several RF lines was created for each transmitted wave.

A. Static Medium

The positions of the scatterers were randomly distributed. To simulate static tissue, the positions of the scatterers within the medium were unchanged for all the simulations.

A series of ultrasound waves having phases φ^k within the range of 0° to 360° were transmitted (φ_0 was set as 0° for simplicity). Every two RF frames from transmitted waves with increasing phase shifts were summed to provide one RF_{sum} frame. To obtain the frequency spectra of RF_{sum} frames, that is the averaged frequency spectrum of the RF lines making up the frame, the fast Fourier transform (FFT) was applied. The spectrum amplitudes were normalized to the fundamental amplitude of a single-pulse response. Fig. 1 shows the fundamental and second-harmonic amplitude, averaged within a 20% bandwidth, of the spectra of the final RF_{sum} frames versus increasing phase shifts.

In Fig. 1, the fundamental and second-harmonic amplitudes show periodicity with increasing phase shift. For the value of 0° phase shift, the fundamental and second-harmonic amplitudes of the RF_{sum} frame are double the amplitudes obtained from one single pulse, so there is an improvement of about 6 dB for both fundamental and second-harmonic amplitudes. For the values of 180° phase shift, the fundamental is the minimum and the second harmonic is the maximum. This strategy corresponds to PI. For the phase shift values of 90° or 270° , the second harmonic passes through the minimum. This corresponds to SHI. To clearly describe PI and SHI and compare the

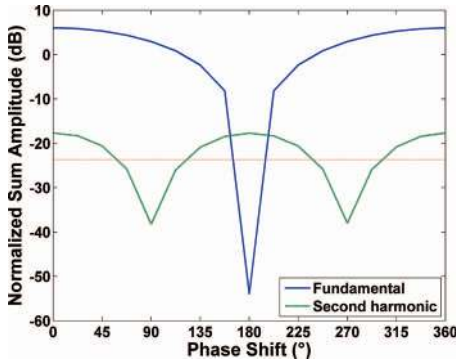


Fig. 1. Simulated average fundamental (dark line) and second-harmonic (light line) amplitudes of RF_{sum} frames versus transmitted phase shifts, obtained on a static medium. The RF_{sum} frames were summed from two RF frames corresponding to two transmitted waves with phase shift ranging from 0° to 360° . The amplitudes were normalized to the averaged fundamental amplitude of a single-pulse response. The dotted horizontal line is the amplitude of the second harmonic of a single-pulse response.

two methods, the spectrum of the RF frame corresponding to a single transmitted pulse and that of the RF_{sum} frame corresponding to two pulses with a 90° or 180° phase shift are drawn together in Fig. 2. In Fig. 2, the fundamental amplitude of PI is reduced to about -55 dB, whereas the second-harmonic amplitude is increased by 6 dB; the fundamental amplitude of SHI is increased by 3 dB, whereas the second-harmonic amplitude is reduced. Both Figs. 1 and 2 obviously show that PI reduces the fundamental frequency and emphasizes the second harmonic, whereas SHI reduces the second harmonic.

B. Medium With Motion

Here, the influence of scatterer motion is investigated. For different simulations, the axial positions of scatterers were changed to simulate the scatterer motion in the wave propagation direction. The displacement profile was simu-

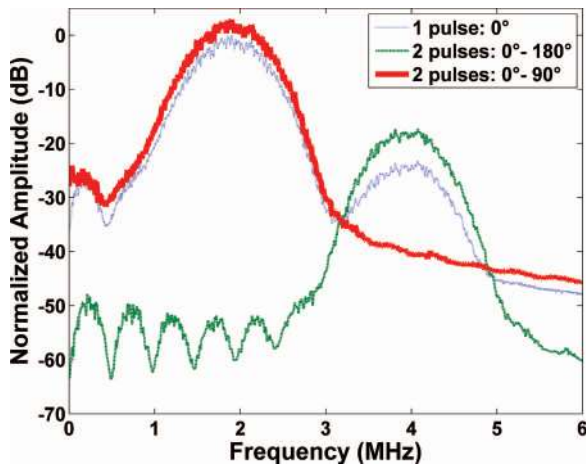


Fig. 2. Simulated spectra of the single (dotted line) and summed RF frame corresponding to PI (thin line) or SHI (thick line), obtained on a static medium. The amplitudes were normalized to the maximum amplitude of a single-pulse response.

lated as a rectangular pattern or a parabolic pattern, and the mean displacement ranged from 0 to λ .

The RF frame corresponding to the pulse with 0° phase was created first, then the displacement of moving scatterers was set, and the second pulse with the phase of 90° or 180° was transmitted to create the second RF frame. After that, the two RF frames were summed as one RF_{sum} frame. For each RF_{sum} frame containing the mean displacement ranging from 0 to λ , the spectrum amplitudes were calculated as in the simulation part A, except that these average RF spectra were calculated only for RF lines covering the moving scatterers, instead of the whole frame as in simulation part A.

Figs. 3(a) and 3(b) correspond to the simulations with a constant scatterer displacement profile, meaning that all the scatterers are moving with the same velocity [see Fig. 4(a)]. Fig. 3(a) presents the fundamental and second-harmonic amplitudes versus the increasing scatterer motion, corresponding to the two 180° phase-shifted transmissions, whereas Fig. 3(b) shows the results corresponding to the two 90° phase-shifted transmissions. These two curves demonstrate that the amplitudes change periodically with increasing scatterer motion. The period is 0.5λ for fundamental frequency and 0.25λ for the second harmonic. In Fig. 3(a), when there is no scatterer motion, the fundamental amplitude is the minimum and the second-harmonic amplitude is the maximum. When the scatterer motion is 0.25λ , both the fundamental and second-harmonic amplitudes are maximum. In Fig. 3(b), the second-harmonic amplitude in a one-pulse image is -24 dB. In a summed image, when no scatterer motion is applied, the second harmonic is reduced from -24 dB to -37 dB, meaning that the second harmonic is reduced by about 13 dB. However, with a scatterer motion of 0.125λ , the second harmonic is increased from -24 dB to -18 dB. That is, the second harmonic can be increased by about 6 dB with the scatterer motion, instead of being reduced with static scatterers.

To show a more realistic situation, a parabolic scatterer displacement profile, similar to the blood velocity profile in a vessel, was also simulated and the results are presented in Figs. 3(c) and 3(d). These two curves also demonstrate that the amplitudes change periodically with increasing scatterer motion. However, for this parabolic profile, the period observed is 0.3λ for fundamental frequency and 0.15λ for the second harmonic. These simulation results deviate from the results of Figs. 3(a) and 3(b) because the simulated displacements, in the case of parabolic profile, varied in a range from zero to a maximum value in the center. This variation leads to an optimal scatterer motion different from the theoretical results obtained with homogenous displacements. It is also observed that the extent of amplitude variation decreases with increasing scatterer motion, and finally the summed amplitude has a stable increase of 3 dB compared with the amplitude of a single pulse. This observation can be explained by the short signal transmitted (four-cycle pulsed waves) instead of continuous waves in theory. The summation of

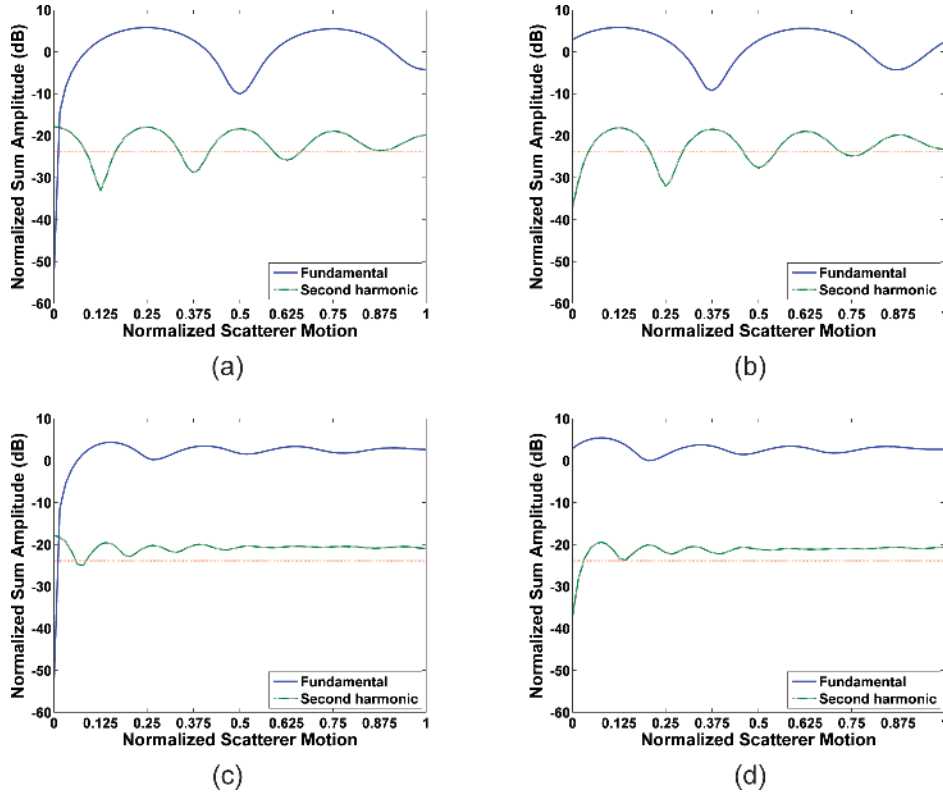



Fig. 3. Simulated average fundamental amplitude (solid line) and second-harmonic amplitude (dashed line) of (a and c) pulse-inversion (PI) imaging or (b and d) second-harmonic inversion (SHI) imaging versus increasing mean scatterer motions (normalized to λ), obtained on moving scatterers. The motion profile was simulated as a rectangular pattern (a and b) or a parabolic pattern (c and d). The amplitudes were normalized to the averaged amplitude of a one-pulse fundamental image. The horizontal dotted line is the amplitude of a one-pulse second-harmonic image. 

the two phase-shifted signals has a specific effect (PI or SHI) only on the superimposed signal portion. Therefore, when large scatterer motion is considered, the superimposed signal portions are small and the observed effects become ineffective. Theoretically, with four-cycle pulses, a scatterer motion equivalent to 2λ or more leads to two backscattered pulses having no common parts in their summation, and therefore PI or SHI effects cannot be observed. Then, the power of the summed signal is twice the power of a single signal, so the amplitude of the summed signal is increased by a factor of $\sqrt{2}$ (3 dB) compared with a single signal.

Figs. 1 and 3 illustrate that the ultimate backscattered harmonic amplitudes are defined by two parameters: the phase shift of transmitted waves and the motion of scatterers. Therefore, the motion can be regarded as an additional phase shift to the original transmitted phase shift as described by (8) and (9). Note that the ultrasound imaging principle is based on the forward and backward propagation of the wave, so the value of scatterer motion should be doubled to be translated into a phase shift.

Fig. 4(b) is a simulated second-harmonic image. Fig. 4(c) presents the PI image with the moving scatterers, whose displacement profile is parabolic, within the width from -5 mm to 5 mm and static scatterers in the surrounding medium. These scatterers moved in the axial direction, and the displacement between the two frames

involved in the PI image is 0.15λ . This displacement in the central part corresponds to the maximum amplitude of the summed signal, whereas the static scatterers in the surrounding area cancel the fundamental amplitude [Fig. 3(c)]. Fig. 4(d) presents the SHI image with a scatterer motion of 0.075λ in the central part and static scatterers all around. This displacement corresponds to the maximum second-harmonic amplitude of the summed signal, whereas the surrounding static scatterers result in a minimum second-harmonic amplitude [Fig. 3(d)]. Both Figs. 4(c) and 4(d) show that the region with the scatterer motion is much brighter than the surroundings without scatterer motion. These simulation results visually show that the scatterer motion greatly influences the resulting images.

IV. EXPERIMENTAL RESULTS

A. Tissue-Mimicking Phantoms

Experiments were first carried out on tissue-mimicking phantoms to validate the response of static nonlinear media insonated by multi-pulses with different phase shifts. The tissue-mimicking phantom imaged was made from 4% agar gel and 0.75% silica particles in water. The open ultrasound platform UlaOp (Microelectronics System De-

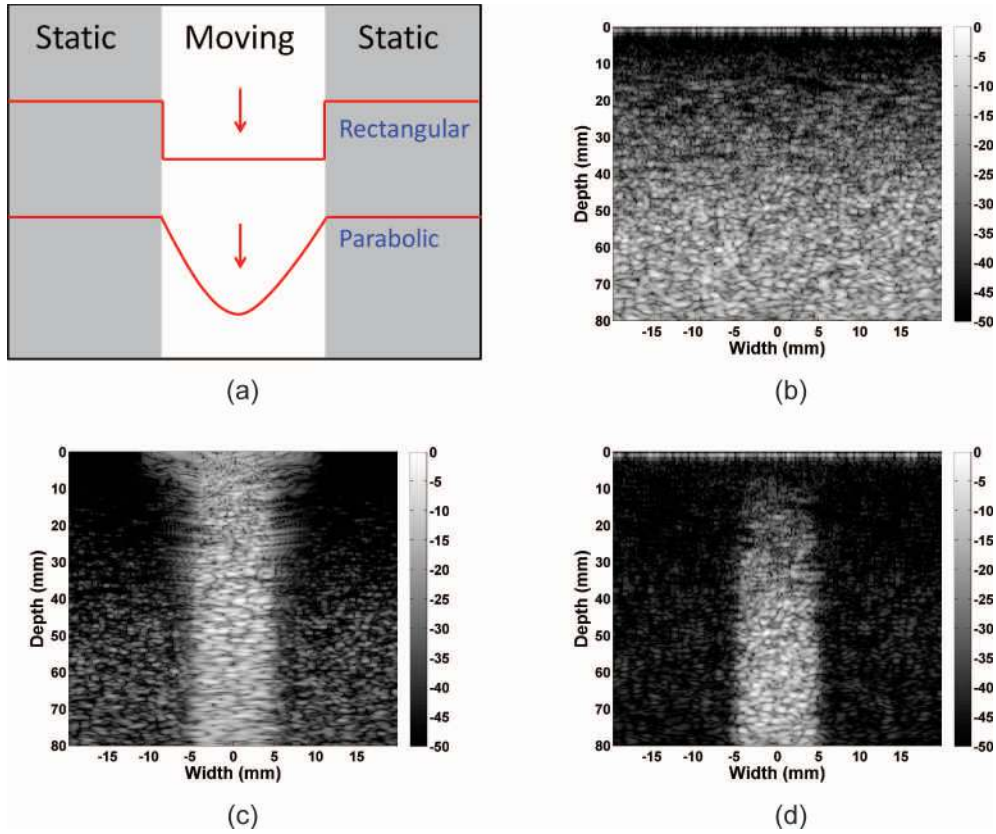


Fig. 4. (a) Schematic diagram of scatterer displacement profile: rectangular (upper) or parabolic (lower) pattern. (b) Simulated standard second-harmonic image, (c) pulse-inversion (PI) image and (d) second-harmonic inversion (SHI) image with axial scatterer motion within the width between -5 mm and 5 mm and static scatterers all around. In the central part of the images, the scatterer motion followed a parabolic profile, and the mean axial motion was (c) 0.15λ or (d) 0.075λ . For the SHI image, an eighth-order Butterworth filter with a bandwidth from 3.6 to 4.4 MHz was used to filter the second harmonic.

sign Laboratory, Florence, Italy) equipped with an LA523 linear probe (Esaote, Genova, Italy) was used to transmit several pulses with various phases [31], [32]. The probe has a 7 -MHz central frequency and a -6 -dB fractional bandwidth of about 100% . Transmitted pulses were a 5 -MHz sine with a Hanning envelope and 7 cycles. The focal point was set at 20 mm.

The two responses corresponding to transmitted pulses with a phase shift ranging from 0° to 180° were summed (φ_0 is set as 0° for simplicity). Fig. 5 shows the averaged amplitudes of first- and second-harmonic bands of the resulting signals versus increasing phase shifts. The averaged amplitudes were calculated as in the simulation, part A.

The experimental results given in Fig. 5 are in agreement with the simulation results shown in Fig. 1: at 0° phase shift, both the fundamental- and second-harmonic amplitudes are increased by 6 dB; at 90° phase shift, the second-harmonic amplitude is reduced by 5 dB; at 180° phase shift, the fundamental amplitude is reduced by 21 dB. The extent of fundamental- and second-harmonic amplitude reductions depend on the amplitudes of the signals generated in tissue, which are mainly determined by the transmitted energy, the nonlinearity of the tissue, and the depth of the ROI.

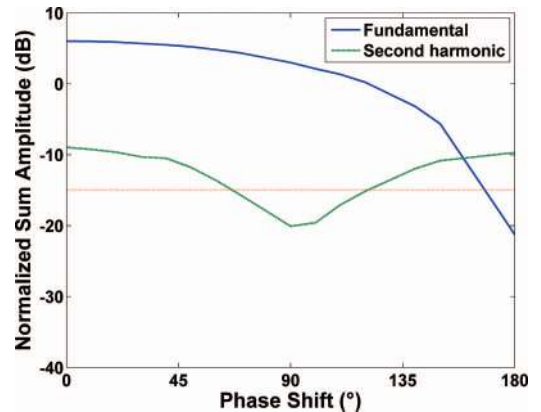


Fig. 5. Experimental average fundamental (solid line) and second-harmonic (dashed line) amplitudes of summed RF signals versus increasing transmitted phase shifts, obtained on a tissue-mimicking phantom. The summed RF signals came from two RF signals corresponding to two transmitted waves with different phase shifts ranging from 0° to 180° . The amplitudes were normalized to the averaged fundamental amplitude of a single pulse response. The horizontal dotted line is the second-harmonic amplitude of a single pulse response.

B. A Single Bubble and a Population of Bubbles Moving in the Axial Direction

To investigate the influence of scatterer motion on multi-pulse imaging techniques, experiments on circulating contrast agents were also carried out. Fig. 6 shows the schematic diagram of the experimental setup: the net hydrostatic pressure resulting from the height difference forced a water flow from the water tank to the capillary fiber. The capillary fiber was made of regenerated cellulose and had an external diameter of 200 μm . The BR14 UCA bubbles (Bracco, Geneva, Switzerland), whose mean diameter is 3 μm , were injected with a syringe.

A single-element piezoelectric transducer, with a central frequency of 3 MHz, 70% fractional bandwidth, and a focal distance of about 70 mm, was connected to an ultrasonic bubble behavior testing (BBT) controller (Microelectronics System Design Laboratory) [33]. The BBT controller made it possible to transmit arbitrary waveforms, to record the signals backscattered from UCA, and to set the PRF, the region of interest (ROI), and the storage data size. The transmitted signals were Tukey-windowed (0.1 tapering ratio) 10-cycle sine pulses with a central frequency of 2 MHz and 170 kPa peak negative pressures. The PRF was 7.81 kHz. For each transmitted wave, the RF signals backscattered from UCA were converted to 2048 digital samples with 14-bit resolution at a 64-MHz sampling rate. Pulses with 0° and 90° phases were transmitted alternately, and the received RF signals were stored. These RF data were used to investigate the relation of bubble motion and the second-harmonic amplitude of SHI.

In the experiments, with the fixed PRF and the steady flow velocity, to emulate various scatterer motions between

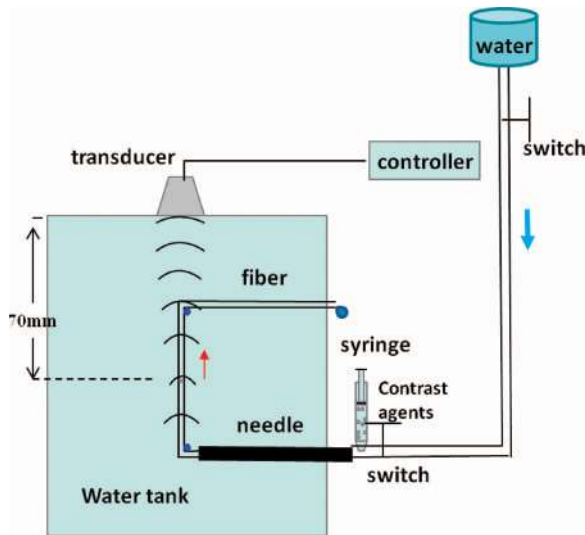


Fig. 6. Schematic diagram of the experimental setup using a single-element transducer. A water flow was created to force the BR14 ultrasound contrast agent (UCA) to circulate inside the fiber (200 μm diameter). The bubble behavior testing (BBT) controller defined the transmitted signal pattern.

90° phase-shifted transmissions, the RF data from one 0° transmission and the RF data from different nonsuccessive 90° transmissions were summed to become different SHI data sets. Fig. 7(a) summarizes the process to obtain different SHI data sets from only one acquisition data set. To avoid confusion with the PRI used during the acquisition, the time interval between the pulses used to get the SHI data sets is termed PRI_{SHI} . After obtaining the SHI data set, second-harmonic amplitudes were calculated in the frequency domain through the FFT. Fig. 7(b) presents the calculation process. The second-harmonic amplitudes of the two 90° phase-shifted RF data were calculated and averaged to give the classic second-harmonic amplitude. The second-harmonic amplitude of SHI was then normalized to the classic second-harmonic amplitude.

To obtain the response of a single bubble, the UCA was diluted to a very low concentration (in the range of 4×10^5 and 7×10^5 microbubbles/mL). The very high sensitivity of the BBT system allows us to obtain the weak echo signal of a single event, and it is assumed that this single event comes from a single bubble (Fig. 8). Fig. 8(a) shows the Hilbert transformation of the RF data (M-mode image) with 0° phase transmissions of a moving single bubble. The residual oscillations of the envelope come from the second harmonic present in the bubble echo. The bubble velocity was measured, from this M-mode image, to be 3.85 ± 0.02 cm/s. Fig. 8(b) shows the second-harmonic amplitude of SHI (normalized to the classic second-harmonic amplitude) versus PRI_{SHI} from various SHI data sets. For each SHI data set, the average value and the standard deviation of the second-harmonic amplitudes are presented. The PRI_{SHI} was also translated to the ratio of bubble motion to transmitted wavelength. Fig. 8 clearly shows that the second-harmonic amplitude of SHI varies periodically with bubble motion, and the maximum value occurs when the bubble motion is 0.126λ . Note that the theoretical maximum value is obtained with a displacement of $\lambda/8$ (or 0.125λ), so Fig. 8 shows an excellent agreement with the theoretical maximum value.

The experimental results obtained on a population of circulating bubbles, with a concentration in the range of 4×10^8 and 7×10^8 microbubbles/mL, are shown in Fig. 9. The maximum bubble velocity was measured to be 6.69 ± 0.3 cm/s from two different approaches (Doppler and water flow capacity measurements with the assumption of a parabolic flow). It should be noted that the bubbles' velocity profile differs from the water velocity profile: it is found that bubbles behave like the red blood cells in a vessel [34] having a slightly flat velocity profile, compared with the parabolic profile [35]. Considering that the maximum velocity is the same for bubbles and water (as proved by the maximum Doppler shift measurements with bubbles), the mean bubble velocity is estimated to be between the mean velocity (3.345 ± 0.3 cm/s) and the maximum velocity (6.69 ± 0.3 cm/s) of the parabolic water flow. Fig. 9 presents the second-harmonic amplitude of SHI (normalized to the classic second-harmonic amplitude) versus PRI_{SHI} from various SHI data sets. For each SHI data set,

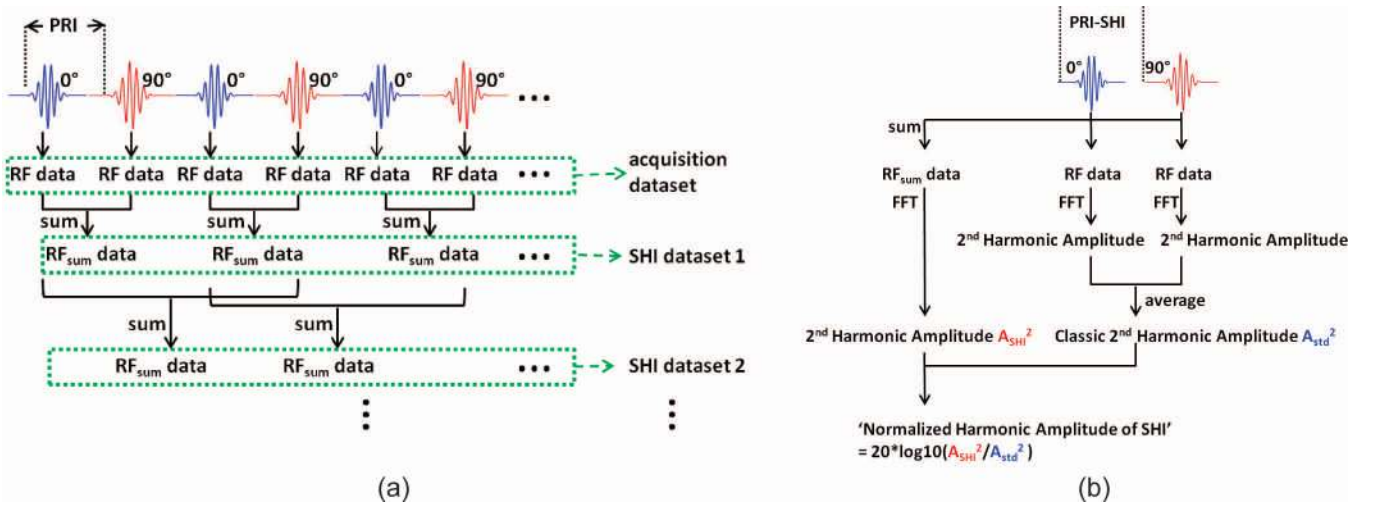


Fig. 7. Schematic diagram of the post-processing for the experiments using a single-element transducer. (a) Different second-harmonic inversion (SHI) data sets were obtained by combining nonsuccessive RF data acquired with the fixed pulse repetition frequency (PRF). (b) The calculation process of the second-harmonic amplitude of SHI.

the average value and the standard deviation of the second-harmonic amplitudes are presented. The PRI_{SHI} was also translated to the ratio of bubble motion to transmitted wavelength. For this translation, the mean water flow velocity (3.345 cm/s, assuming a parabolic flow) was used.

The results show that the second-harmonic amplitude of SHI varies periodically with increasing PRI_{SHI} . The maximum averaged second-harmonic amplitude of SHI is about 5 dB, and the minimum is about -7 dB at the beginning of the curve when a small motion is considered. Therefore, the difference of SHI amplitude reaches 12 dB. Furthermore, the amplitude is less than 0 dB when the PRI_{SHI} is lower than about 0.04λ and greater than 0 dB otherwise. These experimental results show that the effectiveness of SHI varies according to the bubble motion in the UCA region. Therefore, if the flow velocity is low, the PRF must be low enough and the PRI_{SHI} high enough (higher than 0.04λ , according to this experiment) to guar-

antee an efficient SHI (second-harmonic amplitude of SHI in the region of moving bubbles greater than 0 dB).

The first cycle of the curve in Fig. 9 (PRI_{SHI} less than 0.18λ) is more interesting to consider. At first, it corresponds to the lower PRI_{SHI} values; therefore, the two backscattered signals used as the SHI pulses experience fewer transmitted pulses in between. Consequently, the resulting signals mainly reflect the influence of the bubble motion, rather than other influences coming from the transmissions. Second, in practical use, lower PRI_{SHI} is preferred, under the premise of the same effectiveness, to shorten the image acquisition time.

In Fig. 9, the maximum harmonic amplitude first appears when bubble motion is about 0.09λ , whereas in theory, the maximum harmonic amplitude should first appear when the bubble motion is 0.125λ . This deviation comes from the fact that the mean water flow velocity was used to calculate the bubble displacement. Considering that

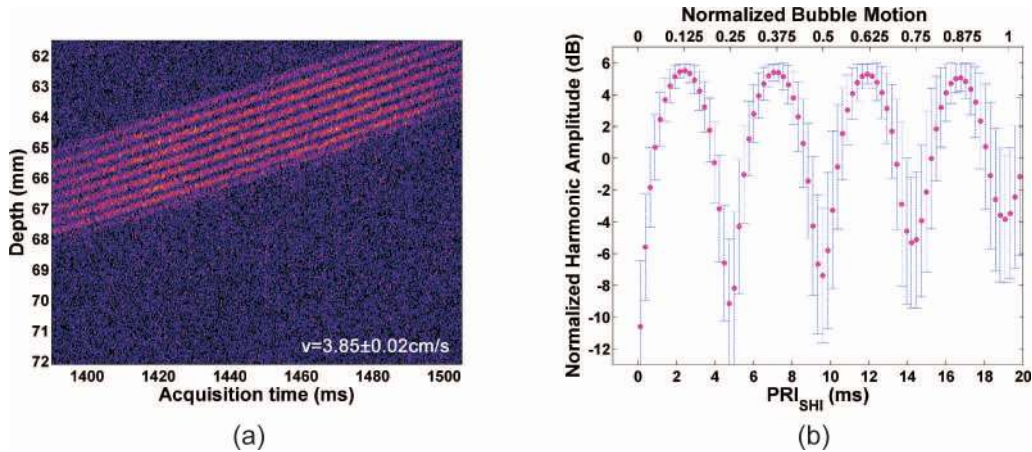


Fig. 8. (a) Experimental M-mode image of a moving single bubble; (b) average (dots) and the standard deviation (bars) of the second-harmonic amplitude of second-harmonic inversion (SHI); normalized to the classic second-harmonic amplitude and expressed in decibels versus pulse repetition interval (PRI) between two 90° phase-shifted pulses (lower axis) or versus the bubble motion, normalized to the transmitted wavelength (upper axis), obtained from the single bubble.

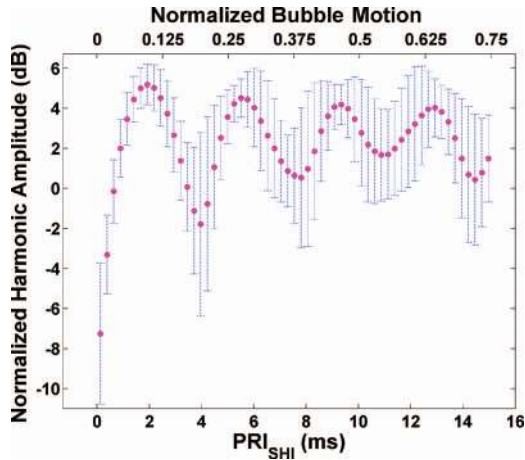



Fig. 9. Experimental average (dots) and the standard deviation (bars) of the second-harmonic amplitude of second-harmonic inversion (SHI; normalized to the classic second-harmonic amplitude and expressed in decibels) versus pulse repetition interval (PRI) between two 90° phase-shifted pulses (lower axis) or versus the bubble motion, normalized to the transmitted wavelength (upper axis), obtained from a population of circulating bubbles. 

bubbles, like the red blood cells in a vessel, tend to have a higher velocity than the velocity described by a parabolic flow when the bubbles are close to the fiber walls [36], their real mean velocity would be greater than the mean water flow velocity and lower than the maximum water flow velocity. Therefore, the actual bubble motion should be within the range of 0.09λ and 0.18λ . These experimental results also agree with the simulation results of the parabolic pattern in the simulation, part B.

C. Flow Phantom Mimicking a Blood Vessel

This section presents the experimental results obtained on a flow phantom. A flow phantom model 453 (Dansk Fantom Service, Frederikssund, Denmark) was imaged. The Sonovue UCA (Bracco, Geneva, Switzerland) diluted in water at a concentration of $0.09 \mu\text{L}/\text{mL}$ was circulating within the tubes embedded in the flow phantom. The tube has a diameter of 8 mm and a tilt angle of 35° . The average velocity of the flow in the tube can be controlled.

The UlaOp open platform, associated with a PA230 phased-array probe (Esaote, Italy), was used to transmit pulses. The probe has a 2.1-MHz central frequency. The transmitted pulses were seven-cycle and 1.7-MHz sine with the Hanning envelope. The peak transmitted pressure was measured as $134 \pm 9 \text{ kPa}$, using a PVDF hydrophone (Precision Acoustics, Dorset, UK). Pulses with 0° and 90° phase were transmitted for the SHI implementation. The imaging depth was 80 mm and the focal point was set at 65 mm. The received pair of successive signals corresponding to transmitted 90° phase-shifted pulses were summed and filtered at the second-harmonic band to form SHI images. The PRF_{SHI} was regulated to obtain SHI images with various bubble motions.

Fig. 10 shows the second-harmonic images (a and c) and SHI images (b and d) acquired with two different PRF_{SHI} values when the nominal mean flow velocity of the flow phantom was $8.3 \pm 0.7 \text{ cm/s}$. The values of PRF_{SHI} were 6 kHz (a and b) and 0.432 kHz (c and d). The dynamic range of these images was 45 dB. For each image, the CTR was calculated as the ratio of the averaged amplitude in the UCA region and in the tissue region and was expressed in decibels. The CTR difference between the SHI image and the corresponding harmonic image was calculated as

$$\Delta\text{CTR} = \text{CTR}_{\text{SHI}} - \text{CTR}_{\text{Harmonic}}. \quad (12)$$

Fig. 10(d) exhibits a much better contrast than Fig. 10(b). When PRF_{SHI} is 6 kHz, the CTR is decreased from 22 dB in the second-harmonic image to 17 dB in the SHI image. However, when the PRF_{SHI} is 0.432 kHz, the CTR is increased from 23 dB in the second-harmonic image to 36 dB in the SHI image. That is, ΔCTR is increased from -5 dB [difference between Fig. 10(b) and Fig. 10(a)] when the PRF_{SHI} is 6 kHz, to 13 dB [difference between Fig. 10(d) and Fig. 10(c)] when the PRF_{SHI} is 0.432 kHz; the improvement of ΔCTR reaches 18 dB. This observation shows that with moving bubbles, the effect of SHI imaging varies according to the PRF_{SHI} of the transmitted pulses. Therefore, the SHI imaging effect can be guaranteed and further improved by controlling the PRF_{SHI} , when the flow velocity is known.

To clearly state the CTR improvement of the SHI method with various PRF_{SHI} values, the curves of the CTR difference between the SHI image and the corresponding harmonic image versus various PRI_{SHI} values is presented in Fig. 11(a) for four different nominal mean flow velocities: 2.8, 5.5, 8.3, and 12.7 cm/s (standard deviation, 0.7 cm/s). Note that these velocity values were given by the manufacturer of the flow phantom. The PRI_{SHI} is also translated to the ratio of bubble motion relative to the transmitted wavelength in Fig. 11(b). This translation is not based on the nominal flow velocity of the flow phantom but considers the projection of the flow velocity component in the wave propagation direction (axial direction). For each PRF_{SHI} , 10 SHI images were acquired; the average value and the deviation of ΔCTR were calculated. The four resulting curves exhibit similar shapes, demonstrating the effectiveness of increasing the CTR of the SHI image by controlling the PRF_{SHI} . For the four different velocities, although the best ΔCTR occurs at different PRI_{SHI} , it always occurs when the bubble motion is translated to be around 0.075λ . The best averaged ΔCTR is about 12 dB. In theory, the maximum ΔCTR value occurs when bubble motion is 0.125λ . This mismatch comes from the deviation between the predefined mean water flow velocity and the actual bubble mean velocity. Several other error sources can also be identified: the actual profile of the flow and the radiation force resulting from the successive transmissions, slightly modifying the bubble velocities [37].

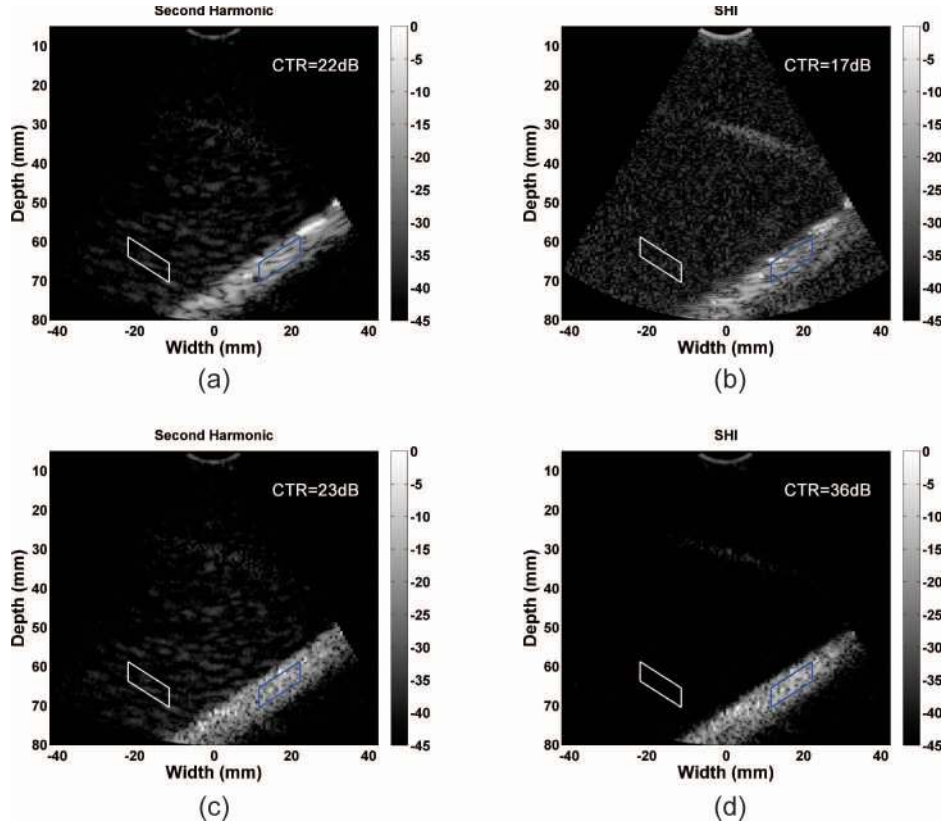



Fig. 10. Acquired experimental (a and c) second-harmonic images and (b and d) second-harmonic inversion (SHI) images of a flow phantom with circulating ultrasound contrast agent (UCA) using a phased-array probe. The pulse repetition frequency (PRF) was (a and b) 6 kHz or (c and d) 0.432 kHz. The nominal average flow velocity was 8.3 ± 0.7 cm/s. For each image, the contrast-to-tissue ratio (CTR) was calculated between the averaged amplitude in the UCA region and in the tissue region. 

In Fig. 11, the results presented are limited to bubble motion from 0 to 0.16λ , instead of several periods shown in the simulations and B experiments. On one hand, to favor short acquisition time, it is less meaningful to investigate greater bubble motion. For example, with the 2.8-cm/s flow velocity, the greatest bubble motion corresponded to a PRF_{SHI} as low as 73 Hz. On the other hand, this curve exhibits the greatest ΔCTR for a bubble motion lower than 0.16λ .

V. DISCUSSION

The effectiveness of the SHI technique depends on the preservation of the second harmonic of SHI in the UCA region and the reduction of the SHI second harmonic in the tissue region. The experimental results reveal that the effectiveness of SHI can be degraded when imaging is performed on relatively slow blood flow because the sum of the UCA second harmonic coming from the two 90° phase-shifted transmissions is also largely reduced. Based on our hypothesis, the ratio of the second-harmonic amplitude of the SHI pulse to the second-harmonic amplitude of a single pulse reaches the maximum value when the bubble motion is around $\lambda/8$, where λ is the wavelength of the transmitted waves. Therefore, the effective preservation,

or even improvement, can be achieved by properly matching the bubble motion and the wavelength of the transmitted wave.

Similarly, with PI, when the bubble motion between the two 180° phase-shifted transmissions is around $\lambda/4$, the additional phase shift of the two received pulses is π for the fundamental frequency and 2π for the second harmonic. Therefore, the final amplitudes scattered from bubbles are maximum—that is, the CTR is maximum. However, in this situation, the resolution is lower than the PI resolution without bubble motion, because the fundamental amplitudes in the UCA region are greatly increased, rather than only second-harmonic signals for PI without bubble motion.

To increase the UCA-scattered signals to optimize the PI or SHI technique, two alternatives can be proposed: adapt the phase of the second transmission or regulate the PRF. However, adapting the phase of the second transmission alters the surrounding tissue responses at the same time. Therefore, to keep the tissue signals reduced, and also for easier implementation, regulating the PRF is the preferable way to perform the optimization.

To optimize these techniques by regulating the PRF, the axial component of scatterer motion is used. Therefore, knowledge of the flow velocity and the angle between the flow direction and the wave propagation direction is

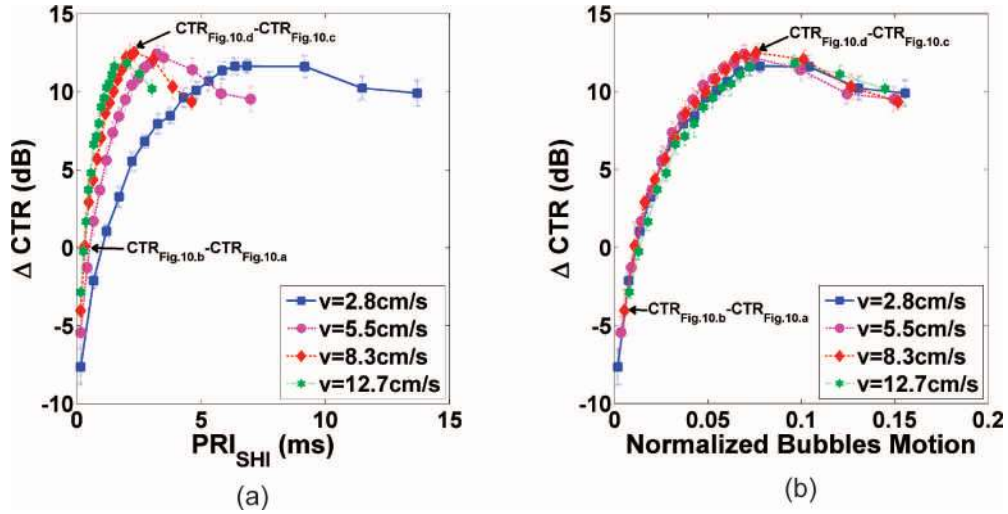



Fig. 11. Experimental contrast-to-tissue ratio (CTR) difference between second-harmonic inversion (SHI) images and corresponding harmonic images ($\Delta\text{CTR} = \text{CTR}_{\text{SHI}} - \text{CTR}_{\text{Harmonic}}$) versus (a) the pulse repetition interval (PRI) and (b) the bubble motion, normalized to the transmitted wavelength, obtained on a flow phantom with circulating ultrasound contrast agent (UCA). For each pulse repetition frequency (PRF), 10 SHI images were acquired to calculate the average value and the standard deviation of ΔCTR . The results for four flow velocities are presented. 

required. The average value of flow velocities in the direction of wave propagation within the ROI can be used, considering that the flow velocities are not uniform and that the wave propagation directions vary within the ROI in phased-array scanning. The lateral component of scatterer motion is neglected because the phase shift of the backscattered signals is much less sensitive to the lateral scatterer motion [38].

However, the use of axial component of scatterer motion to optimize multi-pulse techniques is also restricted by the following condition: the optimal PRI should be found before all the bubbles leave the ultrasound beam, otherwise the backscattered signals directly become uncorrelated and the periodical curves such as those observed in Figs. 8 or 9 cannot be found. This condition can be expressed by the equation:

$$v \cdot \text{PRI} \cdot \sin(\phi) < B, \quad (13)$$

where v is the flow velocity, PRI is the pulse repetition interval, ϕ is the angle between the flow and wave propagation direction, and B is the lateral beamwidth. Taking SHI, for example, based on equation (11), the optimal PRI_{SHI} occurs when

$$\frac{4\pi v \cos(\phi)}{\lambda \cdot \text{PRF}_{\text{SHI}}} = \frac{\pi}{2}. \quad (14)$$

That is,

$$\text{PRI}_{\text{SHI}} = \frac{\lambda}{8v \cos(\phi)}. \quad (15)$$

By substituting (15) into (13), the following condition is deduced:

$$\frac{\lambda \tan(\phi)}{8} < B. \quad (16)$$

Therefore, in case of SHI, the optimization by regulating PRF is feasible when $\lambda \tan(\phi)/8 < B$. For example, in the experiments described in Section IV-C, $\lambda \tan(\phi)/8$ was about 0.162 mm and B was about 1 mm, so the condition was satisfied.

Usually, radiologists using ultrasound systems in clinical applications have prior knowledge of the average velocity range of the blood flow in a ROI. For the implementation of SHI in ultrasound systems, a function can be added to command the preferred PRI_{SHI} range according to λ and the velocity range given by the operators. Consequently, the final optimal PRI_{SHI} can be decided by the operator based on visual preference, by regulating the PRF within the preferred PRI_{SHI} range. If the flow velocity and the direction angle are unknown, the PRF can be adjusted either manually or by the implementation of a recursive function to automatically determine the optimal PRI_{SHI} , using the CTR as the image quality criterion. Doppler is also an option to measure the flow velocity and help in adjusting PRI_{SHI} . The technique can also be implemented in addition to standard fundamental imaging or harmonic imaging that is used to ensure the presence of contrast, while SHI imaging is used to improve the CTR in a ROI.

The proposed method of adjusting PRF has been presented in the paper when steady flows are concerned. However, in many applications, a pulsatile flow can be observed. In this case, although it is not possible to adjust the PRF for all the time-varying velocities, a severe degradation of the technique can be avoided through an adjustment of the PRF according to the average velocity of the pulsatile flow.

All the experiments presented in this study consider static surrounding tissue. Tissue motion is always a limi-

tation for multi-pulse techniques because the harmonics generated as a result of moving tissue cannot be totally canceled, and the increased amplitude in background leads to a reduced CTR [39].

In the theoretical and simulation sections, the UCA is simply assumed to be a nonlinear medium for phase-shifted transmissions, not taking into account effects such as resonance and cavitation. However, the experimental results using BR14 and Sonovue bubbles demonstrate that the responses of the UCA to phase-shifted transmissions and the influence of bubble motion agree with the assumptions, when pulses with several cycles were transmitted. Note that these assumptions should also be tested with shorter pulses.

VI. SUMMARY AND CONCLUSION

In ultrasound imaging, the contrast between UCA and tissue, that is the competition result between the echoes scattered by bubbles and tissue, is a very important criterion to judge contrast detection efficacy. To increase the discrimination between the two media, several multi-pulse techniques have been previously proposed, for example using phase modulation, amplitude modulation or combined phase and amplitude modulation. Some techniques attempt to increase the harmonics produced by UCA while eliminating the linear responses within the transducer bandwidth, where tissue is regarded as linear scatterers [16], [20], [22]. Some techniques take into account the nonlinear wave propagation in tissue and reduce the tissue-generated harmonics within the harmonic bandwidth [18].

However, for any multi-pulse technique, the bubble motion between the transmitted pulses has an inevitable influence and can alter the results of the techniques, especially for those using phase modulation. Therefore, all the multi-pulse techniques in contrast imaging should take into account the influence of this motion. Most of the previous studies reported in the literature regarded bubble motion as a limitation for their multi-pulse techniques. In fact, for some techniques such as SHI, bubble motion can become a positive factor for the technique's effectiveness.

This paper assumes that: 1) for multi-pulse techniques, the phase shift of the echoes backscattered from bubbles is dependent on the transmissions' phase shift; and 2) bubble motion adds an additional phase shift and therefore influences the efficiency of multi-pulse techniques. Simulation results on a static medium insonated by transmissions with different phase shifts and on a medium with scatterer motion insonated by transmissions with constant phase shift validate these hypotheses.

The experimental results are mainly based on the SHI technique, which transmits two 90° phase-shifted waves and the summed received echoes are filtered at the second-harmonic band to form SHI images. The PRF_{SHI} is regulated to take into account various bubble motions. The experimental results on a single bubble, obtained with a single-element probe, confirm that when bubbles move in

the wave propagation direction, the second-harmonic amplitude of SHI changes periodically with the increasing bubble motions between two 90° phase-shifted pulses, and the maximum value first appears when the bubble motion is 0.125λ . Experimental results on a population of bubbles with a single-element probe and on a flow phantom with a phased array probe further demonstrate that the SHI image quality can be guaranteed and improved with suitable bubble motion by regulating the PRF_{SHI} , if the flow is not perpendicular to the wave propagation direction. The best CTR improvement reaches around 12 dB when compared with a single-pulse second-harmonic image. All of these experimental results validate that the phase shift of the echoes backscattered from bubbles is dependent on the transmissions' phase shift, and shows how the bubble motion influences the efficiency of a multi-pulse technique.

The results presented in this paper encourage the development of multi-pulse imaging techniques with automatic control of the phase shift between consecutive pulses or of the PRI to optimize the implemented technique and the image quality.

REFERENCES

- [1] R. Gramiak and P. M. Shah, "Echocardiography of the aortic root," *Invest. Radiol.*, vol. 3, no. 5, pp. 356–366, 1968.
- [2] N. De Jong, R. Cornet, and C. Lancee, "Higher harmonics of vibrating gas-filled microspheres. Part one: Simulations," *Ultrasonics*, vol. 32, no. 6, pp. 447–453, 1994.
- [3] N. De Jong, R. Cornet, and C. Lancee, "Higher harmonics of vibrating gas-filled microspheres. Part two: Measurements," *Ultrasonics*, vol. 32, no. 6, pp. 455–459, 1994.
- [4] S. I. Aanonsen, T. Barkve, J. N. Tjøtta, and S. Tjøtta, "Distortion and harmonic generation in the nearfield of a finite amplitude sound beam," *J. Acoust. Soc. Am.*, vol. 75, no. 3, pp. 749–768, 1984.
- [5] F. Forsberg, W. T. Shi, and B. Goldberg, "Subharmonic imaging of contrast agents," *Ultrasonics*, vol. 38, no. 1–8, pp. 93–98, 2000.
- [6] A. Bouakaz, S. Frigstad, F. J. Ten Cate, and N. De Jong, "Super harmonic imaging: A new imaging technique for improved contrast detection," *Ultrasound Med. Biol.*, vol. 28, no. 1, pp. 59–68, 2002.
- [7] S. Krishnan and M. O'Donnell, "Transmit aperture processing for nonlinear contrast agent imaging," *Ultrason. Imaging*, vol. 18, no. 2, pp. 77–105, 1996.
- [8] S. Krishnan, J. D. Hamilton, and M. O'Donnell, "Suppression of propagating second harmonic in ultrasound contrast imaging," *IEEE Trans. Ultrason. Ferroelectr. Freq. Control*, vol. 45, no. 3, pp. 704–711, 1998.
- [9] T. Christopher, "Source prebiasing for improved second harmonic bubble-response imaging," *IEEE Trans. Ultrason. Ferroelectr. Freq. Control*, vol. 46, no. 3, pp. 556–563, 1999.
- [10] K. B. Krishnan and K. E. Thomenius, "Improved contrast ultrasound with tissue harmonic minimizing pulse," *IEEE Trans. Ultrason. Ferroelectr. Freq. Control*, vol. 55, no. 1, pp. 249–253, 2008.
- [11] M. Pasovic, M. Danilouchkine, G. Matte, A. F. W. van der Steen, O. Basset, N. De Jong, and C. Cachard, "Broadband reduction of the second harmonic distortion during nonlinear ultrasound wave propagation," *Ultrasound Med. Biol.*, vol. 36, no. 10, pp. 1568–1580, 2010.
- [12] C. C. Shen, Y. C. Wang, and Y. C. Hsieh, "A feasibility study of tissue harmonic generation with $3f_0$ transmit phasing," in *IEEE Ultrasonics Symp.*, 2007, pp. 1748–1751.
- [13] C. C. Shen, H. W. Wang, and Y. Y. Chiu, "Contrast harmonic detection with chirp excitation in $3f_0$ transmit phasing," *Ultrason. Imaging*, vol. 30, no. 4, pp. 251–261, 2008.
- [14] C. C. Shen and Y. C. Hsieh, "Optimal transmit phasing on tissue background suppression in contrast harmonic imaging," *Ultrasound Med. Biol.*, vol. 34, no. 11, pp. 1820–1831, Nov. 2008.

- [15] C. C. Shen, Y. C. Yang, and W. S. Chen, "Optimal transmit phasing for harmonic-background suppression with bipolar square-wave pulser," *Ultrason. Imaging*, vol. 32, no. 1, pp. 33–47, 2010.
- [16] D. H. Simpson, C. T. Chin, and P. N. Burns, "Pulse inversion Doppler: A new method for detecting nonlinear echoes from microbubble contrast agents," *IEEE Trans. Ultrason. Ferroelectr. Freq. Control*, vol. 46, no. 2, pp. 372–382, 1999.
- [17] P. J. A. Frinking, A. Bouakaz, J. Kirkhorn, T. Cate, J. Folkert, and N. De Jong, "Ultrasound contrast imaging: Current and new potential methods," *Ultrasound Med. Biol.*, vol. 26, no. 6, pp. 965–975, Jul. 2000.
- [18] M. Pasovic, M. Danilouchkine, T. Faez, P. L. M. J. van Neer, C. Cachard, A. F. W. van der Steen, O. Basset, and N. de Jong, "Second harmonic inversion for ultrasound contrast harmonic imaging," *Phys. Med. Biol.*, vol. 56, no. 11, pp. 3163–3180, Jun. 2011.
- [19] K. Morgan, M. Averkiou, and K. Ferrara, "The effect of the phase of transmission on contrast agent echoes," *IEEE Trans. Ultrason. Ferroelectr. Freq. Control*, vol. 45, no. 4, pp. 872–875, Jan. 1998.
- [20] G. A. Brock-Fisher, M. D. Poland, and P. G. Rafter, "Means for increasing sensitivity in non-linear ultrasound imaging systems," U.S. Patent 5,577,505, Nov. 26, 1996.
- [21] B. Haider and R. Y. Chiao, "Higher order nonlinear ultrasonic imaging," in *IEEE Ultrasonics Symp.*, 1999, vol. 2, pp. 1527–1531.
- [22] R. J. Eckersley, C. T. Chin, and P. N. Burns, "Optimising phase and amplitude modulation schemes for imaging microbubble contrast agents at low acoustic power," *Ultrasound Med. Biol.*, vol. 31, no. 2, pp. 213–219, 2005.
- [23] W. Wilkening and M. Krueger, "Phase-coded pulse sequence for non-linear imaging," in *IEEE Ultrasonics Symp.*, 2000, pp. 1559–1562.
- [24] W. Wilkening, B. Brendel, H. Jiang, J. Lazenby, and H. Ermert, "Optimized receive filters and phase-coded pulse sequences for contrast agent and nonlinear imaging," in *IEEE Ultrasonics Symp.*, 2001, vol. 2, pp. 1733–1737.
- [25] N. de Jong, L. Hoff, T. Skotland, and N. Bom, "Absorption and scatter of encapsulated gas filled microspheres: Theoretical considerations and some measurements," *Ultrasonics*, vol. 30, no. 2, pp. 95–103, 1992.
- [26] P. Marmottant, S. van der Meer, M. Emmer, M. Versluis, N. de Jong, S. Hilgenfeldt, and D. Lohse, "A model for large amplitude oscillations of coated bubbles accounting for buckling and rupture," *J. Acoust. Soc. Am.*, vol. 118, no. 6, pp. 3499–3505, Dec. 2005.
- [27] M.-X. Tang and R. J. Eckersley, "Nonlinear propagation of ultrasound through microbubble contrast agents and implications for imaging," *IEEE Trans. Ultrason. Ferroelectr. Freq. Control*, vol. 53, no. 12, pp. 2406–2415, Dec. 2006.
- [28] F. Varray, A. Ramalli, C. Cachard, P. Tortoli, and O. Basset, "Fundamental and second-harmonic ultrasound field computation of inhomogeneous nonlinear medium with a generalized angular spectrum method," *IEEE Trans. Ultrason. Ferroelectr. Freq. Control*, vol. 58, no. 7, pp. 1366–1376, 2011.
- [29] D. Zhang and X. Gong, "Experimental investigation of the acoustic nonlinearity parameter tomography for excised pathological biological tissues," *Ultrasound Med. Biol.*, vol. 25, no. 4, pp. 593–599, May 1999.
- [30] D. Zhang, X. Gong, and X. Chen, "Experimental imaging of the acoustic nonlinearity parameter B/A for biological tissues via a parametric array," *Ultrasound Med. Biol.*, vol. 27, no. 10, pp. 1359–1365, Oct. 2001.
- [31] P. Tortoli, L. Bassi, E. Boni, A. Dallai, F. Guidi, and S. Ricci, "ULA-OP: An advanced open platform for ultrasound research," *IEEE Trans. Ultrason. Ferroelectr. Freq. Control*, vol. 56, no. 10, pp. 2207–2216, Oct. 2009.
- [32] S. Ricci, L. Bassi, E. Boni, A. Dallai, and P. Tortoli, "Multichannel FPGA-based arbitrary waveform generator for medical ultrasound," *Electron. Lett.*, vol. 43, no. 24, pp. 1335–1336, 2007.
- [33] S. Ricci, E. Boni, F. Guidi, T. Morganti, and P. Tortoli, "A programmable real-time system for development and test of new ultrasound investigation methods," *IEEE Trans. Ultrason. Ferroelectr. Freq. Control*, vol. 53, no. 10, pp. 1813–1819, Oct. 2006.
- [34] M. W. Keller, S. S. Segal, S. Kaul, and B. Duling, "The behavior of sonicated albumin microbubbles within the microcirculation: A basis for their use during myocardial contrast echocardiography," *Circ. Res.*, vol. 65, no. 2, pp. 458–467, Aug. 1989.
- [35] E. Logean, L. Schmetterer, and C. E. Riva, "Velocity profile of red blood cells in human retinal vessels using confocal scanning laser Doppler velocimetry," *Laser Phys.*, vol. 13, no. 1, pp. 45–51, 2003.
- [36] G. J. Tangelder, D. W. Slaaf, M. Muijtjens, T. Arts, M. G. oude Egbrink, and R. S. Reneman, "Velocity profiles of blood platelets and red blood cells flowing in arterioles of the rabbit mesentery," *Circ. Res.*, vol. 59, no. 5, pp. 505–514, Nov. 1986.
- [37] H. J. Vos, F. Guidi, E. Boni, and P. Tortoli, "Method for microbubble characterization using primary radiation force," *IEEE Trans. Ultrason. Ferroelectr. Freq. Control*, vol. 54, no. 7, pp. 1333–1345, Jul. 2007.
- [38] C. C. Shen and P. C. Li, "Motion artifacts of pulse inversion-based tissue harmonic imaging," *IEEE Trans. Ultrason. Ferroelectr. Freq. Control*, vol. 49, no. 9, pp. 1203–1211, 2002.
- [39] M. Crocco, M. Palmese, C. Sciallero, and A. Trucco, "A comparative analysis of multi-pulse techniques in contrast-enhanced ultrasound medical imaging," *Ultrasonics*, vol. 49, no. 1, pp. 120–125, Jan. 2009.